Horiyama *et al. Journal of Wood Science* (2022) 68:52
https://doi.org/10.1186/s10086-022-02058-x

Journal of Wood Science

ORIGINAL ARTICLE

Open Access

Combined analysis of microstructures within an annual ring of Douglas fir (*Pseudotsuga menziesii*) by dynamic mechanical analysis and small angle X-ray scattering

Hiroaki Horiyama[1], Keisuke Kojiro[1*], Yoko Okahisa[2], Tomoya Imai[3], Takafumi Itoh[1] and Yuzo Furuta[1]

Abstract

Dynamic mechanical analysis (DMA) and small angle X-ray scattering (SAXS) measurements of water-saturated wood of Douglas fir (*Pseudotsuga menziesii*) in the temperature range of 0 ℃ to 100 ℃ were focused to clarify microstructural changes within an annual ring. The following results were obtained. Thermal softening behavior caused by micro-Brownian motion of lignin was observed in both earlywood and latewood. The peaks of tan*δ* were found at around 95 ℃ for earlywood and at around 90 ℃ for latewood. These results suggested that the structures of lignin in the cell wall were different between earlywood and latewood. SAXS measurements of water-saturated earlywood and latewood in water were performed with precise temperature control. The scattering intensity increased with increasing temperature, indicating that the density of the matrix was reduced at higher temperature. One-dimensional SAXS intensity at the equator, which approximately represents cellulose microfibrils arrangement in the matrix, was intensively analyzed using the WoodSAS model. The result of this model fitting showed that the cellulose microfibril diameter of latewood was higher than that of earlywood. In addition, the value of interfibrillar distance decreased monotonically in the earlywood, while it decreased rapidly in the latewood from 60 ℃ to 90 ℃. The changes in the cellulose microfibril (CMF) diameter and the interfibrillar distance with increasing temperature between earlywood and latewood by SAXS measurement were different. The differences in CMF diameter and inter-fibril distance between earlywood and latewood measured by SAXS also support the hypothesis that lignin structure differs between earlywood and latewood based on the results of DMA measurements.

Keywords: Earlywood, Latewood, Dynamic mechanical analysis, Small angle X-ray scattering, Lignin, Thermal softening, Douglas fir, Water-saturated wood

Introduction

An annual ring is often used as an indicator to determine the material quality of wood. In the case of softwoods, the distinction between earlywood and latewood is clear in most species, and the latewood ratio to annual ring width and the variation of density within an annual ring has long been studied [1–3]. In the case of softwoods, the density of wood increases almost linearly with increasing in latewood ratio to annual ring width [1]. The different densities of earlywood and latewood are related to different cell wall diameters and thickness [2]. Because of the greater density of latewood, the latewood ratio to annual ring width is sometimes used to judge the strength of the wood [3]. Büyüksarı et al. reported that the bending strength, modulus of elasticity in bending, and tensile strength values of latewood were 2.51, 2.31, and 3.24

*Correspondence: kojiro@kpu.ac.jp

[1] Graduate School of Life Environmental Science, Kyoto Prefectural University, Kyoto 606-8522, Japan
Full list of author information is available at the end of the article

times higher than those of earlywood, respectively [4]. The difference in mechanical properties between earlywood and latewood is thought to be mainly due to the difference in density.

Kagawa et al. reported the results of pulse-labeling whole trees to determine how photosynthates in spring, summer, and autumn are used in the formation of both earlywood and latewood. Analysis of intra-annual $\delta^{13}C$ of the tree rings formed after the labeling revealed that earlywood contained photosynthates from the previous year's summer and autumn as well as from the current spring, while latewood was mainly composed of photosynthates from the current year's summer and autumn, although it also relied on stored material in some cases [5]. The variation of components within an annual ring has also been studied. For example, it has been reported that the distribution of lignin varies [6]. Antonova et al. reported that the increments of lignin amount at each development stage of early and late tracheids were different, and lignin deposition occurred in different conditions and with opposite dynamics during early and late xylem formation [7].

There have been many studies on the annual ring structure of coniferous trees, especially the structure of earlywood and latewood [8–11]. The change in physical properties within an annual ring is mostly explained by the difference in density [4]. There are some references to constituents within an annual ring [5–7]. In other words, the microstructure may be different within an annual ring. However, the relationship between microstructural changes and physical properties within an annual ring has not been investigated. In addition, clarifying the relationship between change in microstructure and physical properties within an annual ring will help us understand how trees change their physical properties in response to climate and environmental changes.

As the methods of this study, we focused on the dynamic mechanical analysis (DMA) and small angle X-ray scattering (SAXS) measurements of water-saturated wood in the temperature range of 0 ℃ to 100 ℃. It has been reported those the thermal softening behavior of water-saturated wood changes when the structure of lignin in the cell wall changes [12]. In addition, in recent years, SAXS measurements have been widely used to understand the crystal structure in cell walls [13, 14]. Penttilä et al. used SAXS to study in detail the change in microstructure with increasing or decreasing moisture content. However, the change in the microstructure of water-saturated wood with temperature change has not been investigated. Those measurements will provide detailed information on the relationship between macrostructure changes, i.e., earlywood and latewood, and microstructure, i.e., crystalline and amorphous regions, changes within an annual ring.

In this study, we attempted a combined DMA and SAXS analysis of earlywood and latewood of Douglas fir (*Pseudotsuga menziesii*) in order to clarify microstructural changes within an annual ring.

Materials and methods

Materials

The samples used for measurements were Douglas fir. The sample sizes were 1.2 mm in the radial direction (R), 30 mm in the tangential direction (T), and 1.0 mm in the longitudinal direction (L) for the measurement of dynamic viscoelastic properties, and 1.0 mm (R), 4.5 mm (T), and 8.0 mm (L) for the measurement of SAXS. The schematic diagram of samples is shown in Fig. 1. The

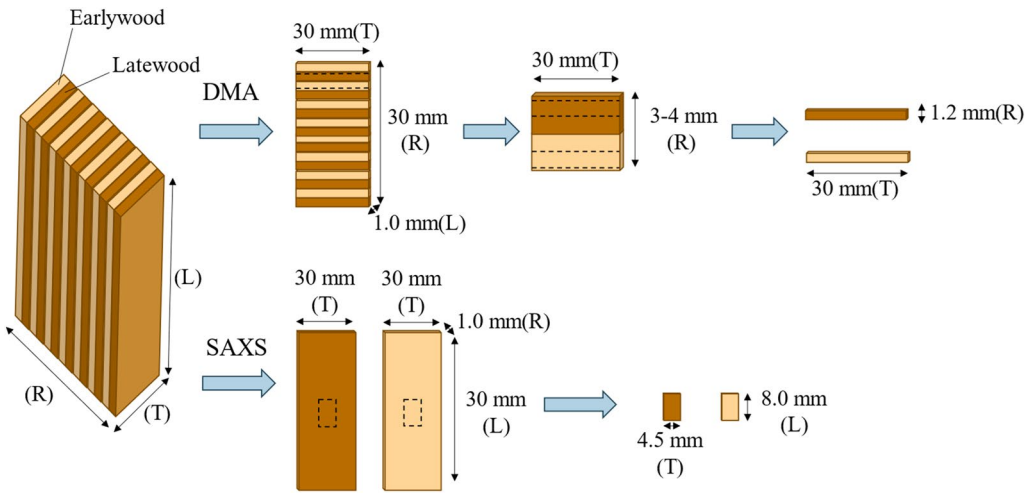

Fig. 1 The schematic diagram of sample shape of dynamic mechanical analysis (DMA) and small angle X-ray scattering (SAXS)

samples were boiled for two hours in distilled water and then annealed to room temperature in those to make them saturated.

Dynamic mechanical analysis (DMA)

Temperature dependence of dynamic elastic modulus (E'), loss modulus (E''), and tanδ were measured by the tensile forced oscillation method using a dynamic mechanical analyzer (DMS6100, Seiko Instruments, Chiba, Japan). The samples swollen by the distilled water were measured in the distilled water at a temperature range of 20 ℃ to 95 ℃. The heating and cooling rate was 1 ℃/min. Frequencies for the measurement were 0.5, 1.0, 2.0, 5.0, and 10 Hz. The span was 12 mm, and the displacement amplitude was 5 μm. The tensile direction was tangential. The schematic diagram of the sample attached to the dynamic mechanical analyzer is shown in Fig. 2. Results were obtained in the second heating process to uniform the heating and cooling histories [15].

Scanning electron microscope (SEM)

The cross-section of the samples was planned using a sliding microtome. The samples were dried at 105 °C for 24 h, and then the cross-section was observed using SEM (TM3030 Plus Miniscope, Hitachi High-Technologies, Tokyo, Japan) at an accelerating voltage of 15 kV. Software ImageJ (National Institutes of Health, USA) was used to measure the cell wall thickness. As for the cell wall thickness, it is the thickness between the cell wall and lumen boundary of two adjacent parenchyma cells or two fiber cells. The distance between the lumens (thickness of two cell walls) of two tracheids was measured, and half of this value was used as the cell wall thickness of the tracheid. The distance was measured at a total of 30 points on the tangential and radial walls, respectively.

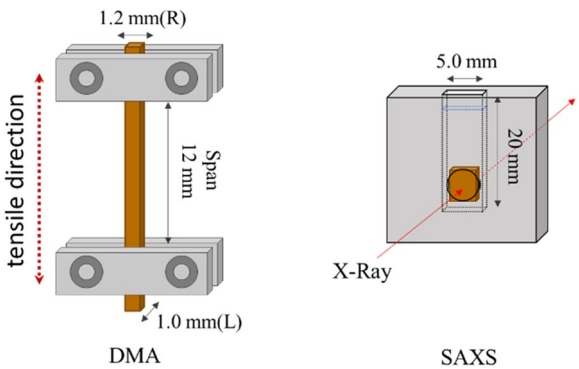

Fig. 2 The schematic diagram of measurement of dynamic mechanical analysis (DMA) and small angle X-ray scattering (SAXS)

Small angle X-ray scattering (SAXS)

SAXS measurements were conducted at a synchrotron facility, BL40B2 beamline in SPring-8 (Hyogo, Japan). The wavelength of X-rays and sample-to-detector distance were set to 1 $Å^{-1}$ and 1.0 m, respectively, which allowed a q range from 0.01 $Å^{-1}$ to 0.7 $Å^{-1}$ to be measured (scattering vector $q = 4\pi\sin(\theta)/\lambda$ with 2θ being the scattering angle). The scattering patterns were recorded with a hybrid pixel counting detector, Pilatus3S 2 M (Dectris Inc., Switzerland). Incident and scattered X-ray flux were counted with ionizing chambers located upstream and downstream of the sample holder, respectively. These two values were used for estimating the absorbance of X-ray by the sample, which was used for the absorbance correction of the scattering data.

The samples had their tangential plane perpendicular to the X-ray beam. The longitudinal direction of the samples was always vertical and perpendicular to the X-ray beam. The specimen swollen by the distilled water was placed in a water-filled liquid cell of stainless steel, which has a beam path of 3 mm and 0.02 mm thickness quartz windows. The liquid cell carrying the sample inside was placed in the sample holder whose temperature was controlled by mK2000 (INSTEC Inc., USA). The schematic diagram of the measurement atmosphere is shown in Fig. 2.

SAXS data analysis

All the data reduction, including camera length calibration by silver behenate, was done using pyFAI [16], a python package for SAXS data reduction. Solvent-subtraction and absorbance correction were made for the two-dimensional scattering pattern at first. Then, the radial integration was performed to obtain the scattering intensity distribution along the azimuth angle (χ-I plot) with the q range of 0.05 ~ 3 $Å^{-1}$, and the azimuth angles where the scattering intensity is the highest and the lowest were searched and found on the χ-I plot. The scattering intensity at the former azimuth, which was defined as the equatorial, was analyzed in this study, while the signal at the latter azimuth was assumed to represent the background scattering derived from the homogeneous structure of the matrix component in the wood cell wall. The azimuthal integration was then performed at each of the azimuths with the maximal and minimal scattering intensity, with an azimuthal range of 15°. The obtained one-dimensional scattering data (q-I plot) at the equatorial were subtracted by the background data at the minimal scattering intensity azimuth.

The background-subtracted equatorial scattering data were analyzed with the WoodSAS model [13], a model based on infinite cylinders in a hexagonal array with

paracrystalline distortion [17] and tailored for wood samples:

$$I(q) = AI_{\mathrm{cyl}}\left(q, \bar{R}, \Delta R, a, \Delta a\right) + Be^{\frac{-q^2}{2\sigma^2}} + Cq^{-\alpha}. \quad (1)$$

In Eq. (1), $I_{\mathrm{cyl}}(q)$ is the intensity from the cylinder arrays with $\bar{R}$ denoting the mean cylinder radius with standard deviation ΔR and a the distance between the cylinders' center points with paracrystalline distortion Δa. The cylinders are assumed to correspond to the cellulose microfibrils (CMFs) [13]. The second term, a Gaussian function centered at $q = 0$ Å^{-1}, approximates the form factor of other unspecified nanoscale features such as pores [13]. The third term of the equation, a power-low at low q with exponent α close to 4, has been assigned to the surfaces of cell lumina [18, 19].

The fitting of Eq. (1) to SAXS data was done using the SasView 4.2.0 software [20] and the WoodSAS model plugin [13]. In the SAXS fits, $\Delta R/\bar{R}$ was fixed to 0.24. The fixing of these parameters was done to accelerate the fitting and to reduce the risk of unrealistic fitting results.

Results

Dynamic mechanical analysis (DMA)

Figure 3 shows the temperature dependence of E', E'', and tanδ in the tangential direction of Douglas fir swollen by water at 0.5 Hz. E' of earlywood and latewood decreased with increasing temperature in the range of 20 ℃ to 100 ℃. E'' of earlywood increased from 10 ℃ to 80 ℃ and then rapidly decreased to 100 ℃. Those of latewood decreased slightly from 10 ℃ to 40 ℃, increased slightly from 40 ℃ to 80 ℃, and then rapidly decreased to 100 ℃. The peaks of tanδ were found at around 95 ℃ for earlywood and around 90 ℃ for latewood. Those peaks, which appear in the range of 0 ℃ to 100 ℃, are attributed to the micro-Brownian motion of lignin [21]. E', E'', and tanδ of latewood were higher than these of earlywood in each temperature. Figure 4 shows the temperature dependence of E'/ρ and E''/ρ in the tangential direction of Douglas fir swollen by water at 0.5 Hz, where ρ is the specific gravity of the sample. It was clarified that the difference in the thermal softening behavior between the earlywood and latewood could not be explained only by the difference in specific gravity.

Scanning electron microscope (SEM)

Figure 5 shows SEM images for the cross-section of Douglas fir used in this study, indicating that the sample is normal wood, neither reaction wood nor starved wood. It was shown that found that there were about 35 cells/mm and about 40 cells/mm in the tangential direction and the radial direction of latewood. It was found that there were about 30 cells/mm and about 20 cells/mm in the tangential direction and the radial direction of earlywood. The tangential and radial wall thickness of latewood averaged 6.10 μm and 8.07 μm, respectively. The tangential and radial wall thickness of earlywood averaged 1.97 μm and 2.04 μm, respectively. Quirk reported

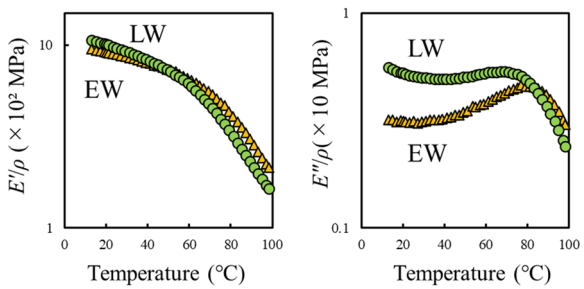

Fig. 4 Temperature dependence of E'/ρ and E''/ρ in tangential direction of Douglas fir swollen by water at 0.5 Hz, where ρ is the specific gravity of the sample. Green filled circles, latewood (LW); orange filled triangle, earlywood (EW)

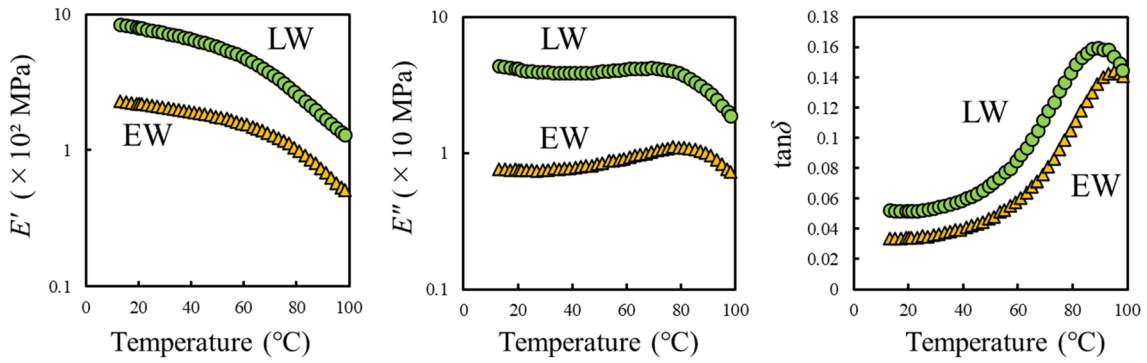

Fig. 3 Temperature dependence of E', E'' and tanδ in tangential direction of Douglas fir swollen by water at 0.5 Hz. Green filled circles, latewood (LW); orange filled triangle earlywood (EW)

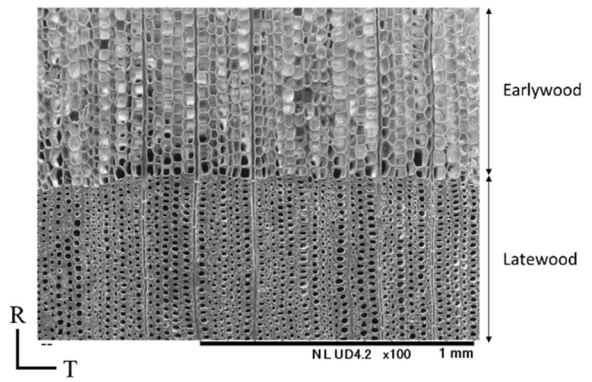

Fig. 5 SEM images on the cross-section of Douglas fir used in this study

that the wall thickness of earlywood and latewood in Douglas fir averaged 2.13 μm and 6.28 μm, which is consistent with the results of this study [22].

Small angle X-ray scattering (SAXS)

SAXS pattern from wood is generally anisotropic as shown in Fig. 6a and b, which is derived from the preferential orientation of CMFs in the secondary wall. The azimuth where the scattering intensity is the highest is called the "equator", and the scattering at this azimuth reflects the density distribution perpendicular to the microfibrils in the secondary wall of wood. We in this study then analyzed the *q-I* plot at the equator, as the distribution of CMFs in the matrix, which is important for wood mechanical property, is represented in the scattering intensity in this direction.

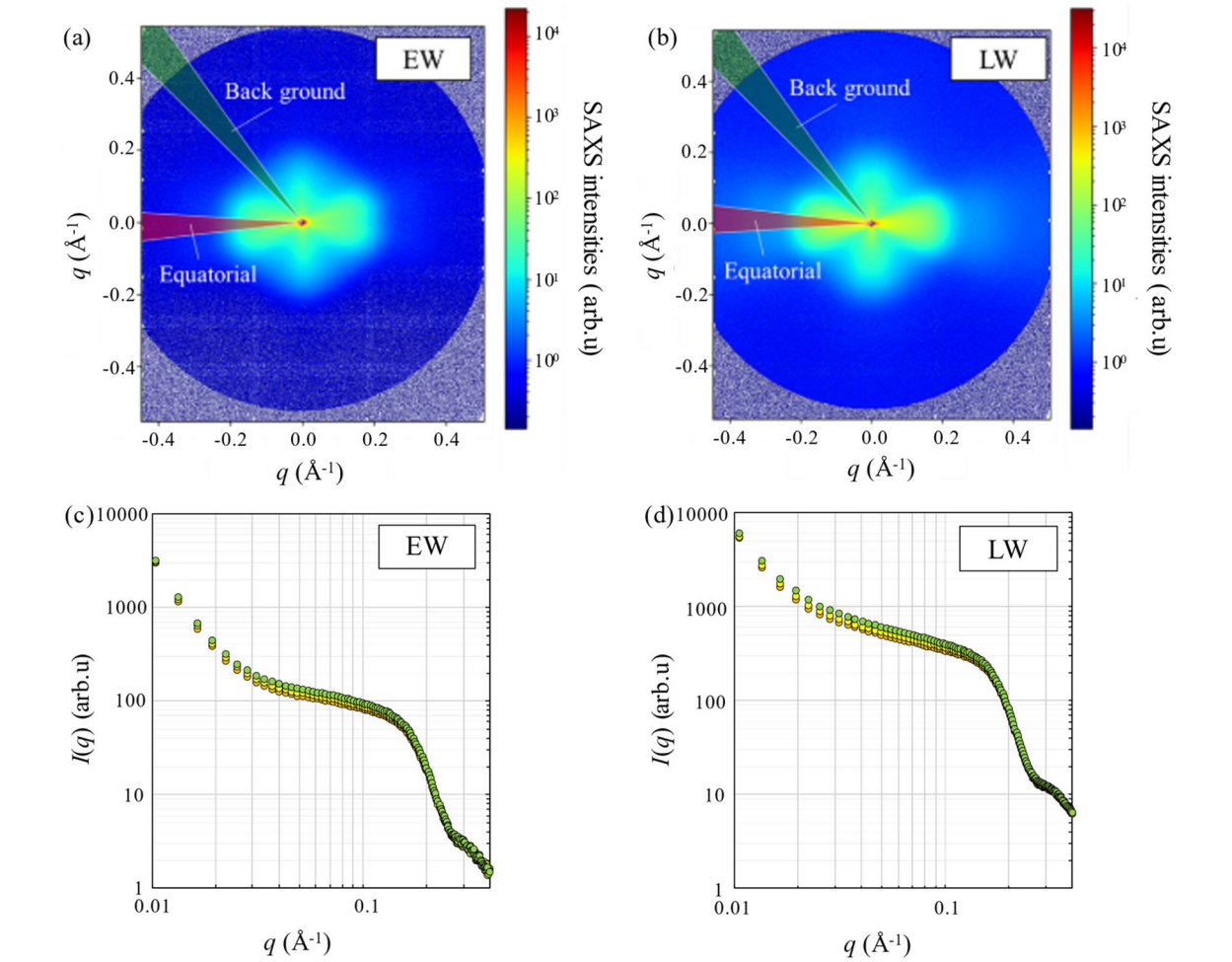

Fig. 6 Representative SAXS data from Douglas fir swollen by water. **a**, **b** The SAXS pattern of earlywood (**a**) and latewood (**b**) in water at 25 ℃, measured at 1.0 m sample-to-detector distance and with the fiber axis vertical. The azimuth ranges for the azimuthal integration at the equator and the background were overlaid on the scattering pattern. **c**, **d** Background-subtracted *q-I* plots for water-saturated earlywood (**c**) and latewood (**d**) in water at 25 ℃ (orange filled circles), 60 ℃ (yellow filled circles), and 90 ℃ (green filled circles)

The scattering intensity at equatorial of latewood was higher than earlywood at all the temperatures tested in this study (25 ℃, 60 ℃, and 90 ℃; Fig. 6c and 6d), indicating the higher density for the latewood whatever the temperature is. More interestingly, the equatorial scattering intensity at the $q < 0.2$ Å^{-1} increases in parallel to the increase of temperature for both earlywood and latewood. This qualitatively indicates that the difference in density between CMFs and matrix components (hemicellulose and lignin) becomes larger at a higher temperature.

For a more detailed analysis of the scattering data, we applied the WoodSAS model for analyzing our data: examples of fitting calculations in WoodSAS analysis are shown in Fig. 7 and the obtained parameters are summarized in Table 1. In the small-angle scattering from wood, the scattering at lower q (< 0.1 Å^{-1}), which is represented by a power law, is governed by the scattering from the lumen surface as discussed already [18, 19], while the information about the microstructure will be more dominant in hither q. For all the temperatures we tested, the exponent in the power law, α for earlywood was close to 4, while α for latewood is strikingly smaller than 4. This implies that the lumen surface in earlywood is approximately smooth, whereas the latewood has a less smooth lumen surface, given the power law rule.

More straightforward parameters, CMFs diameter ($2\overline{R}$) and interfibrillar distance (a) were tracked along with the temperature change, as shown in Fig. 8. Latewood showed higher $2\overline{R}$ and a than earlywood at each temperature, indicating that the width of CMFs and their interval appears to be larger in latewood than earlywood. Similar results were reported for the width of CMFs measured by SAXS, which were similar in earlywood and latewood, or slightly larger in latewood [14]. The differences in the interfibrillar distance (a) between earlywood and latewood become less striking at 90 ℃. Temperature-dependency is also clearly observed for both of these parameters. The higher temperature showed the higher $2\overline{R}$ for both earlywood and latewood, while the smaller a was found for the higher temperature for both earlywood and latewood, indicating that an increase in temperature provided the apparent increase of CMFs in the lateral

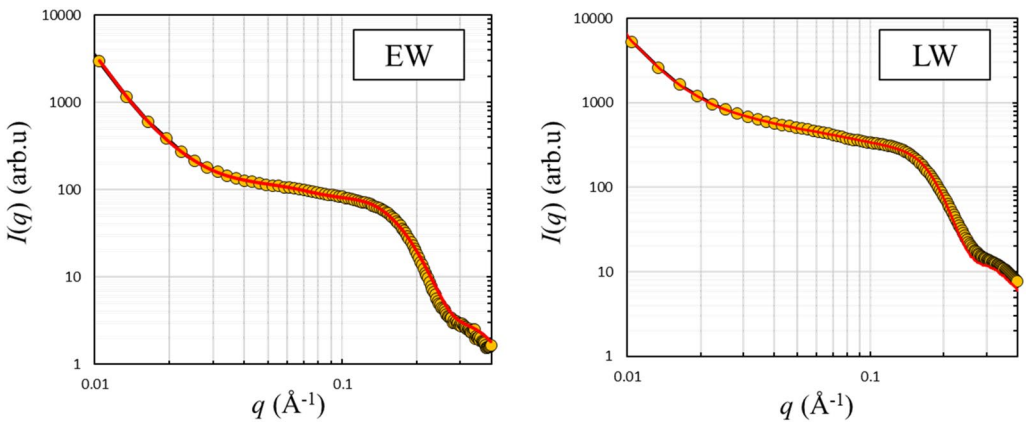

Fig. 7 Representative results of the fitting calculation with the WoodSAS model for the equatorial *q-I* plots for earlywood (EW) and latewood (LW) of Douglas fir swollen by water in water at 25 ℃. The fitted curves were shown by red continuous lines

Table 1 Results of fits to equatorial SAXS intensities from earlywood and latewood of Douglas fir swollen by water

Sample	Temperature (℃)	A ($\times 10^3$)*1	$2\overline{R}$ (nm)*2	$\Delta\overline{R}/R$ *2	a (nm)*2	$\Delta a/a$*2	B ($\times 10^3$) *1	σ ($\times 10^{-2}$)*1	C ($\times 10^{-3}$)*1	α *3
Earlywood	25	0.20 ± 0.01	2.470 ± 0.004	0.24	3.50 ± 0.02	0.465 ± 0.001	0.155 ± 0.022	1.33 ± 0.03	0.012 ± 0.004	4.22 ± 0.06
	60	0.21 ± 0.01	2.485 ± 0.003	0.24	3.48 ± 0.02	0.466 ± 0.003	0.230 ± 0.033	1.31 ± 0.03	0.008 ± 0.001	4.32 ± 0.04
	90	0.22 ± 0.01	2.496 ± 0.014	0.24	3.47 ± 0.03	0.473 ± 0.005	0.201 ± 0.063	1.32 ± 0.01	0.017 ± 0.014	4.20 ± 0.16
Latewood	25	0.93 ± 0.03	2.572 ± 0.002	0.24	3.52 ± 0.00	0.432 ± 0.002	0.181 ± 0.012	1.78 ± 0.04	0.722 ± 0.038	3.43 ± 0.01
	60	0.99 ± 0.04	2.584 ± 0.003	0.24	3.51 ± 0.01	0.433 ± 0.001	0.268 ± 0.010	1.76 ± 0.02	0.460 ± 0.060	3.54 ± 0.03
	90	1.07 ± 0.04	2.603 ± 0.004	0.24	3.47 ± 0.01	0.444 ± 0.002	0.263 ± 0.062	1.85 ± 0.06	1.002 ± 0.546	3.41 ± 0.11

*1 Constants for each term of Eq. (1)

*2 Radius ($\overline{R}$) and distance (a) of hexagonally packed cylinders and their respective coefficients of variation

*3 Exponent of power-law at low q

See Eq. (1) for details

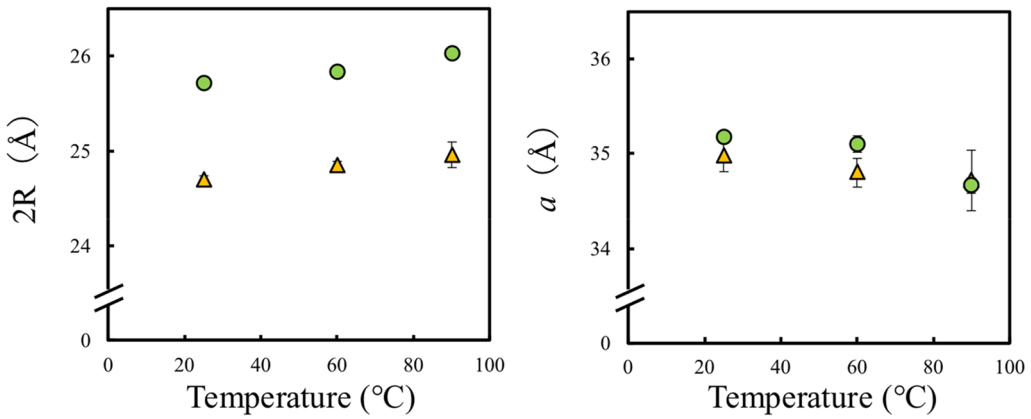

Fig. 8 Plots of the CMF diameter ($2\overline{R}$) and the interfibrillar distance (a) obtained by the fitting calculation with the WoodSAS model, as a function of temperature: orange filled triangles and green filled circles for earlywood (EW) and latewood (LW), respectively. Error bars indicate the standard deviations in the fitting calculation with SasView [20]

direction and a reduction of their intervals. It was noticeable that the a for latewood decreased rapidly from 60 ℃ to 90 ℃.

Discussion

In softwood, the peaks of tanδ are found 80 ℃ to 90 ℃, whereas in hardwood, that is found 60 ℃ to 70 ℃ at 0.05 Hz [15]. Softwood lignin has guaiacyl-propane units, while hardwood lignin has syringyl-propane units in addition to it, and it is generally believed that the degree of condensation of softwood lignin is higher than those of hardwood lignin [23]. These results suggested those the difference in the peaks temperature of tanδ between hardwood and softwood is due to the difference in the cross-linking density derived from the structure of lignin [15]. Since softwood was used in this experiment, the lignin of specimens is thought to have mainly guaiacyl-propane units for both earlywood and latewood. However, it is suggested that the lignin structure, such as cross-linking density, may be different between earlywood and latewood even if the same guaiacyl-propane units are used.

Saka and Thomas reported the distribution of lignin in the cell walls of earlywood and latewood in loblolly pine by bromination technique with the SEM–EDXA system [24]. The lignin concentration of earlywood was 0.20 g/g in the S_2 layer and 0.49 g/g in the compound middle lamella (CML), whereas of latewood, those were 0.18 g/g in the S_2 layer and 0.51 g/g in the CML [24]. It is generally known that the thickness of the S_2 layer is different between earlywood and latewood. Moreover, the fractional volume of the S_2 layer for earlywood and latewood in loblolly pine was 60% and 80%, respectively [24]. In the DMA in the tangential direction, the microfibrils and the matrix of the S_2 layer are arranged in series concerning the tensile direction, so the deformation is considered to be less constrained by the microfibrils [25]. As a result, it is more affected by the quantitatively larger S_2 layer than the quantitatively smaller CML [25]. Therefore, the results of the DMA in the tangential direction strongly reflect the influence of the S_2 layer. As shown in Fig. 5, the density of earlywood and latewood differed greatly, which also suggested those the absolute amount of lignin was different. However, the behavior of E'/ρ and E''/ρ did not match between earlywood and latewood, indicating that the density and the amount of lignin alone cannot explain the difference in thermal softening behavior as shown in Fig. 4. These results suggested that the structure of lignin in the cell wall is different between earlywood and latewood, because the thermal softening behavior, especially tanδ, is different between earlywood and latewood. Since the lignin in both earlywood and latewood is mainly composed of the guaiacyl-propane units, a possible difference in the structure of lignin could be the different number of β-O-4 linkages.

Small angle scattering is one of the structural analyses methods gaining popularity in the field of wood science. For example, Penttilä et al. have studied the relationship between moisture content changes and microstructures changes in wood using X-ray and neutron scattering [13, 14, 26]. In these experiments, in situ measurement plays an important role, which is one of the advantages of small-angle scattering. In this study also, we tracked the structural change of the wood cell wall in the water-saturated state that is occurring in increasing temperature by in situ SAXS measurement. Furthermore, the SAXS data in this study, which were obtained by in situ measurements, are comparable with DMA as shown in Fig. 3.

This means that the insightful interpretation of DMA about the structural change with increasing temperature [15] is now possible to test by the native structural data of SAXS.

The increase in SAXS intensity with increasing temperature as shown in Fig. 6 is considered to be due to the increases in the density difference between CMFs and matrix components. Simply there are two possibilities for this observation: CMF becomes denser, or matrix part becomes sparser with increasing temperature. Given that the thermal expansion of cellulose crystals in wood is very little in the range of 0 °C to 100 °C [27], the latter possibility is a favorable interpretation. The sparser matrix at a high temperature fits the thermal softening of lignin, which has been a well-accepted model [15].

We further tried quantitative interpretation of SAXS data with the WoodSAS model [13], which describes the lateral CMF arrangement in the matrix. Two structural parameters obtained by WoodSAS model seemed to vary in correlation to the DMA result: the increase in $2\overline{R}$ (the diameter of CMFs) and the decrease in a (interfibrillar distance) were observed for the increased temperature or the progress of thermal softening. We believe that these parameter changes are owing to the structural change of the matrix as indicated by DMA and important information to know the change of the matrix in wood cell wall during the thermal softening. However, we in this study do not directly discuss the change of the matrix, as the CMF in the matrix is the direct target of the analysis of the SAXS data in this study.

A simple interpretation for an increase in the CMF diameter ($2\overline{R}$) at higher temperatures is the thermal expansion of cellulose microfibril. However, this is clearly ruled out given the previous report showing that the cellulose crystal in wood hardly expands in the range of 0 °C to 100 °C [27]. We then made an interpretation that this is due to the change of the matrix in the thermal softening, as in the results of the DMA measurements, which then result in an apparent change of CMFs. As discussed above, the matrix of water-saturated wood will become sparser at higher temperatures, which will reduce the electron density of the background or the matrix part. Assuming that the electron density reduction of the matrix is striking only apart from the surface of CMFs but not close to the CMFs, at the temperatures where the thermal softening occurs, the matrix in contact with the CMFs will be more apparent in the matrix background, and accordingly the SAXS signal will represent a larger diameter of the CMFs. This hypothesis could explain the higher value of $2\overline{R}$ at higher temperatures despite no change in the diameter of CMFs themselves. In the future, we would like to perform the similar measurements for the wood samples whose chemical component(s) was/were specifically extracted to demonstrate the thermal softening mechanism with regard to the microstructure of the wood cell wall.

Another parameter, interfibrillar distance (a), showed a monotonous decrease when increasing the temperature from 25 °C to 90 °C. Penttilä et al. reported that in European fir (*Abies alba*) and Norway spruce (*Picea abies*) specimens, the interfibrillar distance decreases by 1–2 nm when drying from near the fiber saturation point to a few percent [14], demonstrating that the distance between CMFs becomes smaller due to the removal of water molecules in drying. We suppose that the similar situation will be found in the wood cell wall at higher temperatures given that the equilibrium moisture content (EMC) of wood cell walls decreases with increasing sample temperature in moisture-saturated wood [28]: the decrease in EMC with a 1 ℃ increase in temperature was estimated to be 0.1% [29]. Thus, one of the apparent changes at higher temperatures is the decrease of the bound water, which consequently results in the decrease of the interfibrillar distance as well as drying. In contrast, it is generally known that the occupied volume of polymers increases with increasing temperature due to the activation of molecular motion [30]. As shown by DMA (Fig. 3), the micro-Brownian motion of lignin is more active at higher temperatures, and then the occupied volume of lignin will be increased, which simply results in a larger distance between the CMFs. In total, in the water-saturated wood at higher temperatures, the increasing and the decreasing trend of the interfibrillar distance might cancel each other, or the decreasing trend (the desorption of bound water) would be slightly more apparent than the increasing trend (the thermal softening of lignin). Although the changes of the interfibrillar distance were not as significant as those of the CMF diameter, it is noticeable that their variation seems to correlate well with tan δ and/or E'' (Figs. 3 and 8).

Earlywood showed a relatively continuous drop of a while latewood showed a small decrease from 25 °C to 60 °C and a rapid decrease from 60 °C to 90 °C. Given that tan δ and E'' reflect the micro-Brownian motion in the amorphous region, this correlation suggests that the temperature-dependent variation of the interfibrillar distance is, in part, owing to the variation of the micro-Brownian motion in the matrix part in the wood cell wall. The difference in the change in the CMF diameter and the interfibrillar distance between earlywood and latewood by SAXS measurement also supported the hypothesis that the lignin structure differs between earlywood and latewood, which was obtained from DMA measurements. Further correlative studies with DMA and SAXS at finer temperature steps will be required for sophisticating this hypothesis. We believe that the direct

comparison between the physical properties clarified by DMA and the structural information by SAXS should be valuable for precisely understanding the structure–function relationship of wood about mechanical and physical properties.

Conclusions

DMA and SAXS measurements were performed on earlywood and latewood of Douglas fir to clarify the relationship between macrostructure and microstructure within an annual ring. The following became clear as those results:

(1) Thermal softening behavior caused by the micro-Brownian motion of lignin was observed in both earlywood and latewood. It was found that the difference in thermal softening behavior between the earlywood and latewood could not be explained only by the difference in specific density. The peak of tanδ was found at around 95 ℃ for earlywood and around 90 ℃ for latewood. These results suggested those the structure of lignin in the cell wall is different between earlywood and latewood.

(2) SAXS measurements of water-saturated earlywood and latewood were performed while the temperature was raised in water, and it was found that the SAXS intensity increased with increasing temperature. The increase in SAXS intensity with increasing temperature is due to the decrease in matrix density caused by thermo-softening of the lignin at high temperatures.

(3) As a result of WoodSAS model-fitting, it was shown that the CMFs diameter of latewood was higher than those of earlywood. It was also found that the CMFs diameter increased in both the earlywood and latewood with increasing temperature. In water-saturated wood at higher temperatures, the increasing and decreasing trends in interfibrillar distance cancel each other out, or the decreasing trend (desorption of binding water) is slightly more pronounced than the increasing trend (thermal softening of lignin), resulting in a slight decrease in the a.

The DMA results indicated that the microstructure differs between earlywood and latewood within an annual ring of Douglas fir. Combined with the SAXS results, it was suggested that the microstructural changes previously mentioned in the DMA results could be observed more directly. Further analyses would be required for a consistent interpretation of these observations.

Abbreviations

DMA: Dynamic mechanical analysis; SAXS: Small angle X-ray scattering; E': Dynamic elastic modulus; E'' Loss modulus; SEM: Scanning electron microscope; CMFs: Cellulose microfibrils; CML: Compound middle lamella; EMC: Equilibrium moisture content.

Acknowledgements

The synchrotron radiation experiments were performed at the BL40B2 of SPring-8 with the approval of the Japan Synchrotron Radiation Research Institute (JASRI) (Proposal Nos. 2019B1176, 2020A1592, 2021A1384). The research was financially supported in part by the Mission-2 research in RISH, Kyoto University.

Author contributions

HH designed the study, collected and analyzed data and wrote the initial draft of the manuscript. KK, TI and YF contributed to dynamic viscoelastic analysis and interpretation of data, and assisted in the preparation of the manuscript. YO and TI contributed to SAXS measurement and SAXS data analysis, and critically reviewed the manuscript. All authors agree to be accountable for all aspects of the work in ensuring that questions related to the accuracy or integrity of any part of the work are appropriately investigated and resolved. All authors read and approved the final manuscript.

Funding

This study is partially supported by a research project of the Mission-2 activity in Research Institute for Sustainable Humanosphere, Kyoto University.

Availability of data and materials

The datasets generated during and/or analyzed during the current study are available from the corresponding author on reasonable request.

Declarations

Competing interests

The authors declare that they have no conflicts of interests.

Author details

[1]Graduate School of Life Environmental Science, Kyoto Prefectural University, Kyoto 606-8522, Japan. [2]Fiber Science and Engineering, Kyoto Institute of Technology, Kyoto 606-8585, Japan. [3]Research Institute for Sustainable Humanosphere, Kyoto University, Uji, Kyoto 611-0011, Japan.

Received: 17 March 2022 Accepted: 12 August 2022
Published online: 02 September 2022

References

1. Kollmann FFF, Côté WA (1968) Principles of wood science and technology, solid wood, vol 1. Springer, Berlin
2. Miller RB (1999) Structure of wood In: Wood Handbook—wood as an Engineering Material (Gen. Tech. Report FPL-GTR113). U.S. Department of Agriculture Forest Products Laboratory, Madison
3. Karlman L, Mörling T, Martinsson O (2005) Wood density, annual ring width and latewood content in larch and Scots pine. Eurasian J For Res 8(2):91–96
4. Büyüksarı Ü, As N, Dündar T (2017) Mechanical properties of earlywood and latewood sections of Scots pine wood. BioResources 12(2):4004–4012
5. Kagawa A, Sugimoto A, Maximov TC (2006) $^{13}CO_2$ pulse-labelling of photoassimilates reveals carbon allocation within and between tree rings. Plant, Cell Environ 29(8):1571–1584
6. Fergus BJ, Procter AR, Scott JAN, Goring DAI (1969) The distribution of lignin in sprucewood as determined by ultraviolet microscopy. Wood Sci Technol 3(2):117–138
7. Antonova GF, Varaksina TN, Zheleznichenko TV, Stasova VV (2014) Lignin deposition during earlywood and latewood formation in Scots pine stems. Wood Sci Technol 48(5):919–936
8. Saiki H (1963) Studies on the annual ring structure of coniferous wood. II. Demarcation between earlywood and latewood (1). Mokuzai Gakkaishi 9(6):231–236
9. Saiki H (1963) Studies on the annual ring structure of coniferous wood. III. Demarcation between earlywood and latewood (2). Mokuzai Gakkaishi 9(6):237–243

10. Saiki H (1965) Studies on the annual ring structure of coniferous wood. IV. Effects of diameter decrease and cell wall thickening of tracheid on latewood formation. Mokuzai Gakkaishi 11(1):1–6
11. Saiki H (1965) Studies on the annual ring structure of coniferous wood. V. Variation from the pith toward outside. Mokuzai Gakkaishi 11(5):185–190
12. Miyoshi Y, Kojiro K, Furuta Y (2017) Lignin from advanced viewpoints in wood physics researches. J Soc Mater Sci Jpn 66(10):697–706
13. Penttilä PA, Rautkari L, Österberg M, Schweins R (2019) Small-angle scattering model for efficient characterization of wood nanostructure and moisture behaviour. J Appl Crystallogr 52(2):369–377
14. Penttilä PA, Altgen M, Carl N, van der Linden P, Morfin I, Österberg M, Schweins R, Rautkari L (2020) Moisture-related changes in the nanostructure of woods studied with X-ray and neutron scattering. Cellulose 27(1):71–87
15. Furuta Y, Nakajima M, Nakatani T, Kojiro K, Ishimaru Y (2008) Effects of lignin on the thermal-softening properties of water-swollen wood. J Soc Mater Sci Jpn 57(4):344–349
16. Ashiotis G, Deschildre A, Nawaz Z, Wright JP, Karkoulis D, Picca FE, Kieffer J (2015) The fast azimuthal integration Python library: pyFAI. J Appl Crystallogr 48(2):510–519
17. Hashimoto T, Kawamura T, Harada M, Tanaka H (1994) Small-angle scattering from hexagonally packed cylindrical particles with paracrystalline distortion. Macromolecules 27(11):3063–3072
18. Jakob HF, Tschegg SE, Fratzl P (1996) Hydration dependence of the wood-cell wall structure in Picea abies. A small-angle X-ray scattering study. Macromolecules 29(26):8435–8440
19. Nishiyama Y, Langan P, O'Neill H, Pingali SV, Harton S (2014) Structural coarsening of aspen wood by hydrothermal pretreatment monitored by small-and wide-angle scattering of X-rays and neutrons on oriented specimens. Cellulose 21(2):1015–1024
20. Doucet M, Cho JH, Alina G, Bakker J, Bouwman W, Butler P, Campbell K, Gonzales M, Heenan R, Jackson A, Juhas P, King S, Kienzle P, Krzywon J, Markvardsen A, Nielsen T, O'Driscoll L, Potrzebowski W, Ferraz LR, Richter T, Rozycko P, Snow T, Washington A (2018) SasView. Version 4:2. https://doi.org/10.5281/zenodo.1412041
21. Furuta Y, Nakajima M, Nakanii E, Ohkoshi M (2010) The effects of lignin and hemicellulose on thermal-softening properties of water-swollen wood. Mokuzai Gakkaishi 56(3):132–138
22. Quirk JT (1984) Shrinkage and related properties of Douglas-fir cell walls. Wood Fiber Sci 16(1):115–133
23. Harada T (1990) Chemistry of wood. Buneido Publisher, Tokyo, pp 69–70
24. Saka S, Thomas RJ (1982) A study of lignification in loblolly pine tracheids by the SEM-EDXA technique. Wood Sci Technol 16(3):167–179
25. Furuta Y, Makinaga M, Yano H, Kajita H (1997) Thermal-softening properties of water-swollen wood. II. Anisotropic characteristics of thermal-softening properties. Mokuzai Gakkaishi 43(1):16–23
26. Penttila PA, Zitting A, Lourencon T, Altgen M, Schweins R, Rautkari L (2017) Water-accessibility of interfibrillar spaces in spruce wood cell walls. Cellulose 28(18):1–15
27. Hori R, Wada M (2005) The thermal expansion of wood cellulose crystals. Cellulose 12(5):479–484
28. Stamm AJ, Harris EE (1953) Chemical processing of wood 76(2):165
29. Stamm AJ, Loughborough WK (1935) Intensely, little attention has been given the thermodynamic aspects of swelling. Colloid Symp Monogr 11:121
30. Bicerano J (2002) Glass transition. Encycl Polym Sci Technol 2:655–677

Publisher's Note